Interacting quantum walks on the 1D Su-Schrieffer-Heeger model

Submitted By

S. Gauthameshwar

School of Physical Sciences

National Institute of Science, Education and Research (NISER), Bhubaneswar

Under the Guidance of

Dr. Tapan Mishra

Reader-F

School of Physical Sciences

National Institute of Science, Education and Research (NISER), Bhubaneswar

Acknowledgement

I am deeply grateful to my supervisors, Prof. Tapan Mishra, for his unwavering support and guidance in introducing me to the fascinating field of quantum simulation of many-body physics. His vast knowledge, open problems, and passion for research have been instrumental in shaping my research interests and inspiring me to pursue my work with enthusiasm.

I also express my gratitude to my Quantum Matter Theory group, who have been instrumental in helping me develop coding skills, mastering literature search, and critically analyzing research papers. My heartfelt thanks go out to my seniors Ashirbad dada, Rajashri (Raju) didi, Biswajit dada, and Soumya dada for their invaluable support in shaping my understanding of the field and guiding me through the research process.

I would like to thank Prof. Kush Saha for his valuable inputs in clarifying my doubts whenever I approached him. I am also indebted to Prof. Pratap Kumar Sahoo for introducing me to my supervisor and providing me with this excellent research opportunity.

Furthermore, I would like to express my appreciation to my juniors Aditya, Krishnaprasad *et al.*, for their intriguing questions and stimulating discussions, which have broadened my perspective on physics.

Last but not the least, I also thank my parents (and Krishnapriya) for being supportive and believing I would become great someday.

S. Gauthameshwar

5th Year Integrated M.Sc.

School of Physical Sciences

NISER, Bhubaneswar

Abstract

The Su-Schrieffer-Heeger(SSH) model is a well-studied system in condensed matter physics that is known for its ability to host topological phases. Recent research has focused on understanding the topological properties of the SSH model in the presence of interactions and quantifying its Chern number. In this thesis, we explore two types of interaction Hamiltonians, the on-site and nearest-neighbor interactions, and quantify the Chern number using quantum walks and methods such as mean chiral displacement and Thouless pumping. Our findings reveal that the on-site interaction induces a quantized Chern number in the SSH model, while the nearest-neighbor interaction exhibits topological signatures in the eigenspectrum and edge-localized states in the quantum walks. To simulate the hardcore nearest-neighbor interaction on the *qiskit* quantum simulator, we designed a quantum circuit using the Trotterization decomposition and found excellent agreement with the exact time dynamics predicted using exact diagonalization. While we have yet to compute the topological invariant of this model, it remains an exciting area of our future work.

Contents

Chapter 1

Introduction to Berryology

Berryology is a field that has emerged in physics recently that deals with the effect of the non-trivial phase a quantum state obtains when it adiabatically traverses through all momentum states in a band. For a long time in physics such phase was considered trivial because it could be shown we can gauge off that additional phase by multiplying appropriate phase[1]. However, Berry in 1984[2] showed this phase can be made a gauge invariant quantity if we come back to the same momentum state we started from (i.e), a closed loop in the parameter space of the adiabatic transformation and named the quantity Berry phase. This is big news for experimentalists since they can now try to find this exotic observable in experiments. For theorists, it is even more dear because the consequence of this phase in physical systems is all now a matter of visualizing geometric curves and surfaces. This makes it beautiful, intuitive and powerful at the same time, being able to explain specialized and complicated science in simpler terms. Berry phase has found applications in explaining several physics such as quantised plateaus in quantum hall effect[3], anomalous velocity in band dispersion of particles in electromagnetic fields[4], modern theory of polarization[5], and adiabatic charge pumping of particles in a lattice[6]. We shall define everything we had said about the Berry phase rigorously below.

1.1 Adiabatic theorem and Berry phase

The adiabatic theorem that says our system will remain in its instantaneous eigenstates (we assume it is initialized to an eigenstate at $t = 0$) if the Hamiltonian is varied slowly. If we define a parametric description of the Hamiltonian by introducing a set of variables $\mathbf{R}(t) = (r_1(t), r_2(t), r_3(t), \ldots, r_n(t))$ that implicitly depend on time that varies so slowly to assume adiabaticity, we can say

$$\hat{H}(\mathbf{R})|n(\mathbf{R})\rangle = E_n(\mathbf{R})|n(\mathbf{R})\rangle \tag{1.1}$$

where $|n(\mathbf{R})\rangle$ is the instantaneous eigenstate of the Hamiltonian at time t, and $E_n(\mathbf{R})$ is its corresponding eigenvalue. The time evolved state of this adiabatic evolution in parameter space is given by:

$$|\psi(t)\rangle = e^{-i\theta(t)}|n(\mathbf{R}(t)\rangle \tag{1.2}$$

where the phase $\theta(t)$ is

$$\theta(t) = \frac{1}{\hbar}\int_0^t E_n(\mathbf{R}(t'))dt' - i\int_0^t \langle n(\mathbf{R}(t'))|\frac{d}{dt'}|n(\mathbf{R}(t'))\rangle dt' \tag{1.3}$$

The first term represents the global phase that trivially appears as an outcome of TDSE. The second term is called as the Berry phase defined as:

$$\begin{aligned}\gamma_n &= i\int_0^t \langle n\left(\mathbf{R}\left(t'\right)\right)\left|\nabla_{\mathbf{R}}\right| n\left(\mathbf{R}\left(t'\right)\right)\rangle \frac{d\mathbf{R}}{dt'}dt' \\ &= \int_{\mathbf{R}_0}^{\mathbf{R}_t} \mathbf{A}_n(\mathbf{R})d\mathbf{R}\end{aligned} \tag{1.4}$$

where we have defined a new term called Berry connection as:

$$\mathbf{A}_n(\mathbf{R}) = i\langle n(\mathbf{R})|\nabla_{\mathbf{R}}|n(\mathbf{R})\rangle \tag{1.5}$$

When we have a closed curve in the parametric space, we can describe the same physics in the form of surface integral over the Berry curvature which is defined as:

$$\mathbf{\Omega}_n = \nabla_{\mathbf{R}} \times \mathbf{A}_n(\mathbf{R}) \tag{1.6}$$

We can define a topological invariant quantity, also known as the Chern number as:

$$C = -\frac{1}{\pi}\oint \mathbf{A}_n(\mathbf{R}).\mathbf{dR} \tag{1.7}$$

1.2 Discrete symmetries and their effects on the Berry phase

1.2.1 Time reversal symmetry

Time reversal is a symmetry that if present in a system says there will be no difference in the governing equation of motion of our system if we play it backwards. In other words, if our system has time reversal then, as $t \to -t$, $x \to x$ and $p \to -p$ with no change in the Schrodinger's equation of our quantum system. The time reversal operator is a product of a unitary U and a conjugation K operator by definition to respect the uncertainty principle in the time reversed frame and is also its own inverse.

$$\hat{\tau} = UK \tag{1.8}$$

The time reversal operation on a Hamiltonian in its momentum basis states:

$$\hat{\tau}H(k)\hat{\tau} = H^*(-k) \tag{1.9}$$

In a Bloch band of a lattice, the Bloch states transform under time reversal symmetry as

$$\hat{\tau}[u_{n,k}(r)] = u^*_{n,-k}(r) = u_{n,k}(r) \tag{1.10}$$

Realizing this symmetry in the Berry connection in Eq.1.5, we have:

$$\begin{aligned}\mathbf{A}_n(k) &\overset{\text{on TR}}{=} i\int d^3\mathbf{r}u_{n,k}(\mathbf{r})\partial_k u^*_{n,k}(\mathbf{r}) \\ &= -i\int d^3\mathbf{r}u^*_{n,k}(\mathbf{r})\partial_k u_{n,k}(\mathbf{r}) \\ &= i\int d^3\mathbf{r}u^*_{n,k}(\mathbf{r})\partial_{-k} u_{n,k}(\mathbf{r}) \\ &= \mathbf{A}_n(-k)\end{aligned}$$

Thus, we can conclude on TR symmetry,

$$\mathbf{A}_n(k) = \mathbf{A}_n(-k) \tag{1.11}$$

The Berry curvature changes under TR as:

$$\mathbf{\Omega}_n(k) = -\mathbf{\Omega}_n(-k) \tag{1.12}$$

1.2.2 Inversion symmetry

Inversion symmetry is a symmetry that is observed about a point (usually the origin). The space is inverted about this point as $r \to -r$ while time remains unchanged. As a result, the momentum $p \to -p$, and no conjugation exists since $t \to t$. the inversion operator acts on the Hamiltonian in momentum space as

$$\hat{\mathcal{I}}H(k)\hat{\mathcal{I}} = H(-k) \tag{1.13}$$

The effect of this operation on the Bloch states enjoying inversion symmetry reads as

$$\hat{\mathcal{I}}[u_{n,k}(r)] = u_{n,-k}(-r) = u_{n,k}(r) \tag{1.14}$$

Following similar calculations as in the case of time reversal symmetry transformation of Berry phase, under inversion symmetry,

$$\mathbf{A}_n(k) = -\mathbf{A}_n(-k) \tag{1.15}$$

Similarly, the Berry curvature transforms as:

$$\mathbf{\Omega}_n(k) = \mathbf{\Omega}_n(-k) \tag{1.16}$$

Under inversion symmetry, we can say that the Berry phase

$$\gamma_n = \oint dk\mathbf{A}_n(k) \overset{\text{on inversion}}{\longrightarrow} \oint dk\mathbf{A}_n(-k) \overset{\text{under symmetry}}{\longrightarrow} -\oint dk\mathbf{A}_n(k)$$

If we use the gauge properties of Berry phase, we have an arbitrary phase of $2m\pi$ with $m \in \mathbb{Z}$ that can be added and still leaves the Berry phase unchanged. So, including this fact we have the effect of this symmetry reading as:

$$\gamma_n = -\gamma_n + 2m\pi \tag{1.17}$$

Eq.1.17 has two solutions: $\gamma_n = 0$ with $m = 0$ and $\gamma_n = \pi$ with $m = 1$. Thus, Berry phase exists as a quantum in systems enjoying inversion symmetry.

1.3 Berry phase in the modern theory of polarization

In condensed matter lattices with infinite extension of the lattice size or finite systems with periodic boundary conditions, the concept of polarization we had been introduced in the classical sense becomes ill-defined. The choice of lattice cell changes the polarization directions while recreating the same lattice, thus making polarization multivalued. In quantum mechanical picture, the integrals over space that is periodic in nature become ill-defined due to unbounded nature of position operators[7]. Thus, the modern theory of polarization came that uses the concepts of Wannier functions to address these anomaly and also be in agreement with the experimental setups that are able to measure this quantity in the form of small currents[8].
Wannier functions are defined as the inverse Fourier transform of the Bloch state that has strong localization properties about a lattice site. The Wannier states is defined in terms of Bloch states as:

$$|w(j)\rangle = \frac{1}{\sqrt{N}} \sum_{k} e^{-ikj} |u_n(k)\rangle \tag{1.18}$$

The expected center of a Wannier state is given as (after some straightforward calculations):

$$\langle w(j)|\hat{j}|w(j)\rangle = \frac{i}{2\pi} \int_{-\pi}^{\pi} dk \, \langle u_n(k) \mid \partial_k u_n(k)\rangle + j \tag{1.19}$$

Thus, multiplying Eq.1.19 by particle charge q, we get the lattice polarization as

$$P = q\langle w(j)|\hat{x}|w(j)\rangle = q\frac{i}{2\pi} \int_{-\pi}^{\pi} dk \, \langle u_n(k) \mid \partial_k u_n(k)\rangle + qj \tag{1.20}$$

The first term in Eq.1.20,

$$P_{\text{electric}} = q\frac{i}{2\pi} \int_{-\pi}^{\pi} dk \, \langle u_n(k) \mid \partial_k u_n(k)\rangle = \frac{q}{2\pi}\gamma_n$$

is the polarization that our system acquires as a result of the Berry phase it possesses. We also notice the second term in Eq.1.20 tells us that we have a polarization lattice that has q shift of each polarization value that are all equivalent. Therefore, our system can acquire a non-trivial topology only if we have a finite Berry phase that introduces a polarization correction which is not $mod(q)$. This follows from the gauge invariance property of γ_n where an addition of an integer multiple of 2π keeps γ_n unchanged, and in $P_{electric}$, an integer multiple of γ_n shifts the polarization value by an integer multiple of q.

Summary

In this chapter, we have been introduced to the necessary concepts of topology that we will repeatedly encounter in the physics of our model. The definition and motivation of Berry phase, how it appears in our system and how it behaves in systems that enjoy certain symmetries were briefly discussed. We have also seen one place in condensed matter physics where Berry phase is used, namely the modern theory of polarization. In our numerical simulations, we will find this precise lattice polarization and hence, the Berry phase using a scheme called *Thouless pumping*. We will also see that the inversion symmetry preserves the topology of the interacting SSH model thus, making edge states possible even in presence of interaction.

Chapter 2

The continuous time quantum walk

2.1 Classical walks and its continuum limit

Physical quantum walks are defined on a directed graph where the vertices play the role of the states our walker can be in, and the directed edges play the role of going from one state to the other. Now in this system, we introduce stochasticity (i,e) the walker takes a decision at each step of the walk and proceeds to the next state depending on the decision he takes. We consider one such stochastic process called the Markov process where the stochasticity is choosing one of the adjacent vertices with a probability corresponding to the weight of the directed edge.

2.1.1 Classical Markov process

A Markov process is a stochastic process that has two main underlying properties:

1. The decision of going to $n+1th$ state from nth state only depends on the decision taken at nth step and *not* on the decisions that he might've taken at previous states.
2. The next state is determined by randomly choosing a directed edge originating from his current state with a probability equal to the weight of the corresponding edge.

Fig.2.1 shows a Markov process with three states and directed edges denoting transition between them. We can describe the state of the walker at time t by a state vector with its ith

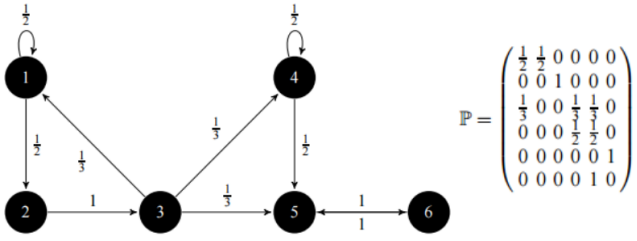

Fig. 2.1: An example of a Markov process with its corresponding transition matrix.

coefficient denoting the probability of being in the ith state.

$$\bar{p}(t) = \begin{bmatrix} p_1(t) \\ p_2(t) \\ \dots \\ p_n(t) \end{bmatrix}$$

Here t can be in steps, or continuous. We start with discrete t and then proceed to its continuum limit. From the second property of Markov processes, we can say the probability of reaching state i at time t is the sum over all possible state j it could've been in time $t-1$ and then jumping to state i with probability T_{ij}. This can be written as:

$$p_i(t) = \sum_j T_{ij} p_j(t-1)$$

So, if we construct a transition matrix T with its coefficient T_{ij} denoting the probability of going from state j to i, we have the recursive stochastic equation:

$$\bar{p}(t+1) = M.\bar{p}(t) \tag{2.1}$$

We observe that the $t+1$th step only depends on its decision in the previous step and not on its far past decisions and so, retains the conditions of a Markov process. Now that we have written the entire process as a linear equation, we can write the state at time t in terms of the state at $t=0$ by using the properties of linear equations:

$$\bar{p}(t) = M^t.\bar{p}(0) \tag{2.2}$$

By taking infinitesimal time steps for an infinitely large amount of times, we get a continuous limit of discrete classical walks defined above. So, under this approximation, we have to introduce a generator matrix H that takes a state $\bar{p}(t) \to \bar{p}(t+\delta t)$.

After some calculations, we end up with the infinitesimal time evolution matrix H as the laplacian of the graph defined:

$$H_{ij} = \begin{cases} d_j & \text{if } i = j \\ -1 & \text{if } i \neq j \text{ and adjacent} \\ 0 & \text{if } i \neq j \text{ and not adjacent} \end{cases} \tag{2.3}$$

with d_j being the number of neighbors vertex j has. The differential equation that governs our time evolution is given by the Master equation of continuous walk:

$$\frac{d}{dt}\bar{p}(t) = -\gamma H.\bar{p}(0) \tag{2.4}$$

where γ is the diffusion rate to nearest neighbors. Eq.2.4 has the solution of $\bar{p}(t)$ as:

$$\bar{p}(t) = e^{-\gamma H t}\bar{p}(0) \tag{2.5}$$

2.2 Quantizatoin of classical random walks: The continuous time quantum walk

Quantising the above Master equation demands us to replace $\frac{d}{dt}$ operator with $i\hbar\frac{d}{dt}$, consider γH as our Hamiltonian, and replace the probability vector by a state vector in the space of lattice sites $|N\rangle$. Assuming $\hbar = 1$, the equation takes the form of Schrodinger equation on quantising:

$$i\frac{d}{dt}|\psi(t)\rangle = \hat{H}|\psi(t)\rangle \tag{2.6}$$

Thus, our unitary time propagator analogous to $M(t)$ becomes:

$$\hat{U}(t) = e^{-i\hat{H}t} \tag{2.7}$$

The quantum analog of Eq.2.5 is given by:

$$|\psi(t)\rangle = e^{-i\hat{H}t}|\psi(0)\rangle \tag{2.8}$$

After time t, the probability of our boson being in state n is given by:

$$p_n(t) = |\langle n|\psi(t)\rangle|^2 = |c_n(t)|^2 \tag{2.9}$$

Summary

In this chapter, we looked into the numerical tool we shall be using extensively to explore the topological properties of our system. Quantum walks can be formulated from classical Markov processes in a graph by considering its continuum limit and then quantising appropriately by respecting uncertainty relation. The time dependent Schrodinger's equation is but a statement of a quantum particle performing quantum walk on a lattice, if the basis is discrete in nature.

Chapter 3

The Su-Schrieffer-Heeger(SSH) model

The SSH model is a toy model that is widely studied in topological models that gives a good intuition and flavor of the concepts of topology seen in a physical system. The basic ideas that we infer from this model can be generalized in higher dimensional lattice models to understand phenomena such as edge conduction in a bulk insulating material.

3.1 The SSH model

The non-interacting SSH model is a tight-binding model that simulates a dimerized lattice chain with an imbalance in the hopping parameter. As shown in Fig.3.1, a dimerized lattice has two sites, A and B, in a primitive cell. This two-site primitive cell can be translated by

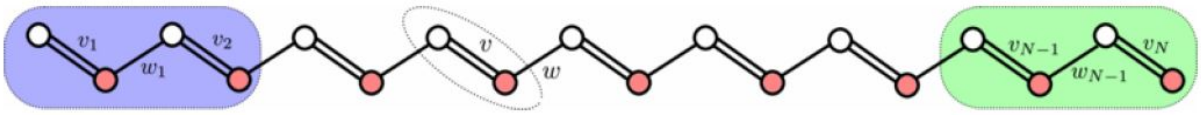

Fig. 3.1: A dimerized lattice chain in 1D that shows imbalance in hopping within its cell v, and between cells w. Site A is shown in white color while site B is shown in orange color[9].

units of lattice constant to define a complete 1D chain. Hopping within a primitive cell that moves particle from site A to B has a hopping strength v, whereas hopping to its next cell has a different hopping strength w. In second quantised formalism, the Hamiltonian of a 1D SSH model by considering the hopping terms, can be given as:

$$\hat{H} = -\sum_i v(\hat{a}_i^\dagger \hat{b}_i + h.c) + w(\hat{b}_i^\dagger \hat{a}_{i+1} + h.c) \tag{3.1}$$

3.1.1 Periodic boundary conditions, topology and the eigenspectrum

If we perform a Fourier transform, move to the momentum space and solve for the eigenvalues and eigenstates, we end up with:

$$E_\pm(k) = \pm|\mathbf{h}(k)| = \pm\sqrt{v^2 + w^2 + 2vw\cos(k)} \tag{3.2}$$

$$|\pm k\rangle = \begin{pmatrix} \pm e^{-i\phi(k)} \\ 1 \end{pmatrix} \tag{3.3}$$

where

$$\phi(k) = Arg(\mathbf{h}(k)) = tan^{-1}\left(\frac{w\sin(k)}{v + w\cos(k)}\right) \tag{3.4}$$

and $h(k)$ comes from the parametric representation of our momentum Blocks of Eq.3.1

$$H(k) = (v + w\cos(k))\sigma_x + w\sin(k)\sigma_y + 0.\sigma_z = \mathbf{h}(k).\sigma \tag{3.5}$$

We get a neat geometric picture of all of our physical quantities in the $h_x - h_y$ plane. The eigen energy is the length of our vector while the phase our momentum state has is the angle the vector makes with respect to the x-axis. The vector $\bar{h}(k)$ in the parameter space is a circle with radius $|w|$ centered at $|v|$ in the $h_x - h_y$ plane. As we vary k within the FBZ, we get $\bar{h}(k)$ as the locus of points that move around this circle.Fig.3.2 shows this geometric visualization. Our momentum states have the topology of a ring in our parametric space. Substituting for $|\pm k\rangle$ from Eq.3.3 in Eq.1.5, we get the Berry connection to be:

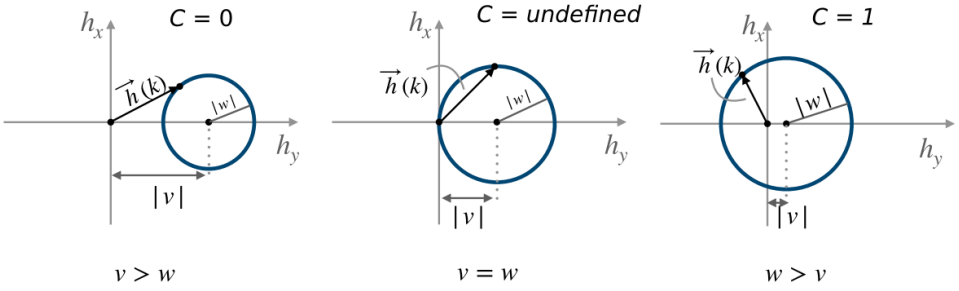

Fig. 3.2: Trajectories followed by $\bar{h}(k)$ as we move around the FBZ. The three cases when $v > w$, $v = w$, and $v < w$ are shown. We get a non-zero winding number when our circle crosses the origin[10].

$$A_{\pm}(k) = -\frac{1}{2}\frac{d\phi(k)}{dk} \tag{3.6}$$

Thus, the Chern number in Eq.1.7 becomes:

$$C = \begin{cases} 0 & \text{if } v > w \\ \text{undefined} & \text{if } v = w \\ 1 & \text{if } v < w \end{cases} \tag{3.7}$$

Thus, we can classify the topology of our model and hence, comment on the Berry phase the model acquires as we traverse through the momentum states adiabatically.

3.1.2 Open boundary conditions, edge states and the eigenspectrum

If we impose open boundaries, we need to numerically solve for the eigenspectrum and plot it to find the behavior of our energy eigenstates.

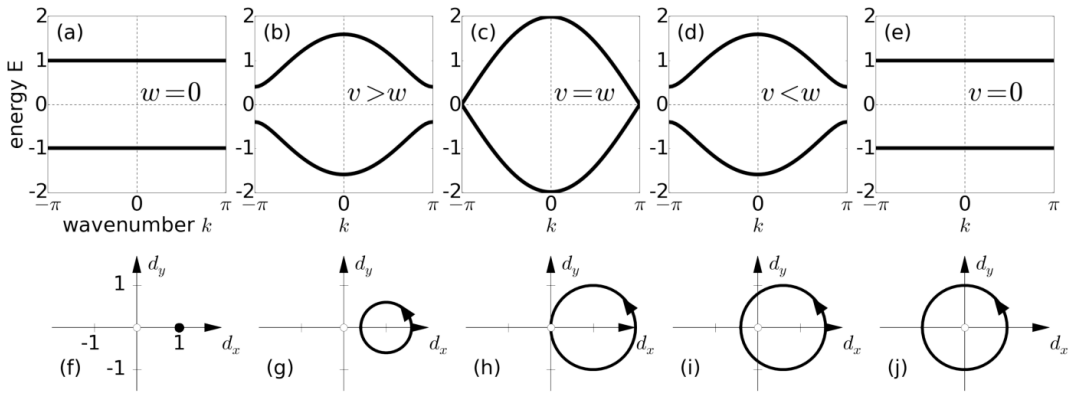

Fig. 3.3: The energy spectrum (a)-(e) and their corresponding topology in the phase space (f)-(j) obtained for various cases of v and w. We see that there is a distinction in the topology of these momentum states even though the eigenvalues seem identical[11].

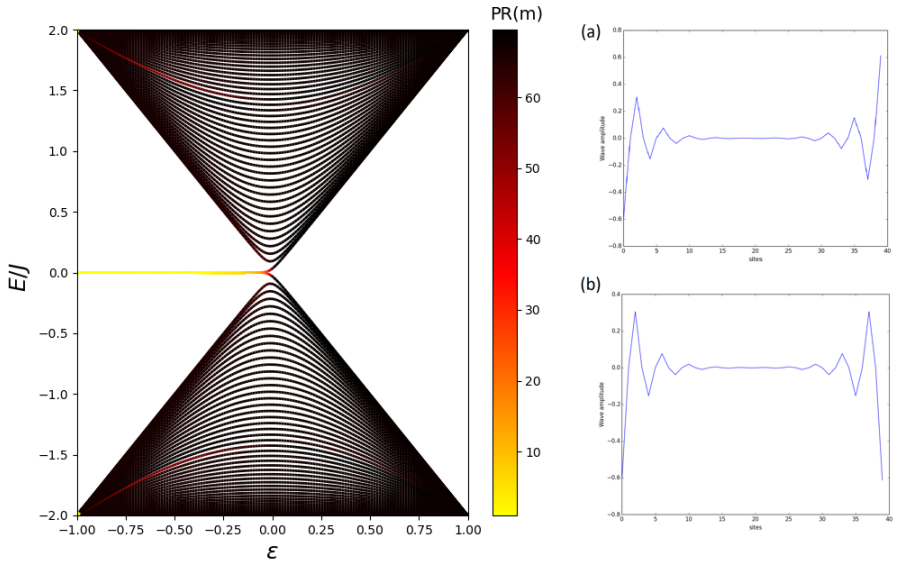

Fig. 3.4: The plot of eigenspectrum(left) and edge states(right) of a single-particle SSH model under OBC for varying ϵ. (a) and (b) shows the eigenstates of the yellow states we see in the eigenspectrum at $\epsilon = -0.5$. The color of these states indicates strong localization and the plot of these eigenstates show they are localized at the edges.

Fig.3.4 shows the eigenspectrum with an alternate definition of the hopping strengths $v = J(1+\epsilon)$, $w = J(1-\epsilon)$. We have a new quantity ϵ, the dimerization whose sign tells us the topological phase of our model and the magnitude tells the strength of such dimerization in the respective phases. The color map is plotted for a quantity known as the *participation ratio* which was proposed by D. J. Thouless [12] in his formulation of localization of electrons in lattices.

$$PR(|\psi_m\rangle) = \frac{1}{\sum_i |\langle i|\psi_m\rangle|^4} \tag{3.8}$$

The quantity is of $\mathcal{O}(N)$ when the state $|\psi_m\rangle$ is a scattering state spread all over the lattice. It is of $\mathcal{O}(1)$ for the localized state since only very few coefficients take part in the sum.
Our SSH model has another interesting symmetry called *Chiral symmetry* which explains the existence of these edge states in pairs. Chiral symmetry or sublattice symmetry states that a lattice with two sites, A and B in a unit cell only talk to the other one and not to itself. In

other words, there is no $A-A$ or $B-B$ bonds in our lattice, only $A-B$ and $B-A$ bonds. The chiral operation by the chiral operator $\hat{\Gamma}$ is defined as

$$\hat{\Gamma} = \sum_{i=1}^{N} \hat{n}_{i,A} - \hat{n}_{i,B} \tag{3.9}$$

with the property that under this symmetry,

$$\hat{\Gamma} H(k) \hat{\Gamma} = -H(k) \tag{3.10}$$

This gives us two important inferences. First, our eigenspectrum is symmetric about $E = 0$ as the Hamiltonian anti-commutes with the chiral operator in Eq.3.10 and for every E there will be an energy $-E$. This also means that if there comes a point where our energy spectrum has $E = 0$, they stick together and exist as a pair. This is the reason why the edge states appear with energy $E = 0$ only when gap closes. Secondly, if our system possesses chiral symmetry, it can be proven the momentum curve will exist only in the $h_x - h_y$ plane (i.e), $h_z = 0$. We have to break chiral symmetry if we wish to go to the topological regime of our SSH model without the band gap closing in the process.

3.2 The interacting SSH model, its eigenspectrum and edge states

In the interacting SSH model, we have primarily studied two types of interaction. The softcore on-site interaction and hardcore nearest-neighbor interaction. Eq.3.11 shows the interacting SSH Hamiltonian. Both of these models possess *inversion symmetry* due to which it is possible for them to have non-trivial topology.

$$\hat{H} = -\sum_{i} v(\hat{a}_i^\dagger \hat{b}_i + h.c) + w(\hat{b}_i^\dagger \hat{a}_{i+1} + h.c) + \frac{U}{2} \sum_{\alpha \in \{A,B\}} \hat{n}_i^\alpha (\hat{n}_i^\alpha - 1) + V\left(\hat{n}_i^A \hat{n}_i^B + \hat{n}_i^B \hat{n}_{i+1}^A\right) \tag{3.11}$$

In Fig.3.5, we see the participation ratio classifying four types of eigenstates. The green and blue colored states have high degree of scattering throughout the lattice space and hence, have high PR. The orange states have partial scattering into the bulk along with edge localization(the fact that these states disappear in the trivial phase also supports this) while the red states are strong bound states caused by the interaction that leads to the formation of repulsively bound pairs. The correlation matrix of the two-particle spectrum will give us better insights to the nature of the types of eigenstates we find in our interacting models. Fig.3.6 elaborates the probability distribution $P(m, n)$ of finding particles at site m and n. (a) and (d) shows the edge-bulk scattering states for $U = 4$ and $V = 4$ respectively. These states are recognised from the feature where the edges of the matrix are significant implying one particle scatters into the bulk while the other gets localized at the edges. (b) and (e) are the scattering edge-edge state where both the particles are scattered to the cornets of the matrix, meaning if one particle is in this edge, the other should be either here or at the other edge. Note that this is precisely the edge states we got in the non-interacting model, thus showing edge localized states are present in the eigenspectrum of both these interacting systems! (c) and (f) are the bound bulk-bulk states. These states are marked by strong diagonal or near diagonal terms, telling us the two particles always tend to be close to each other wherever they exist in the lattice. These are precisely the repulsively bound pairs we will see in our quantum walks when interaction becomes strong enough to overwhelm the

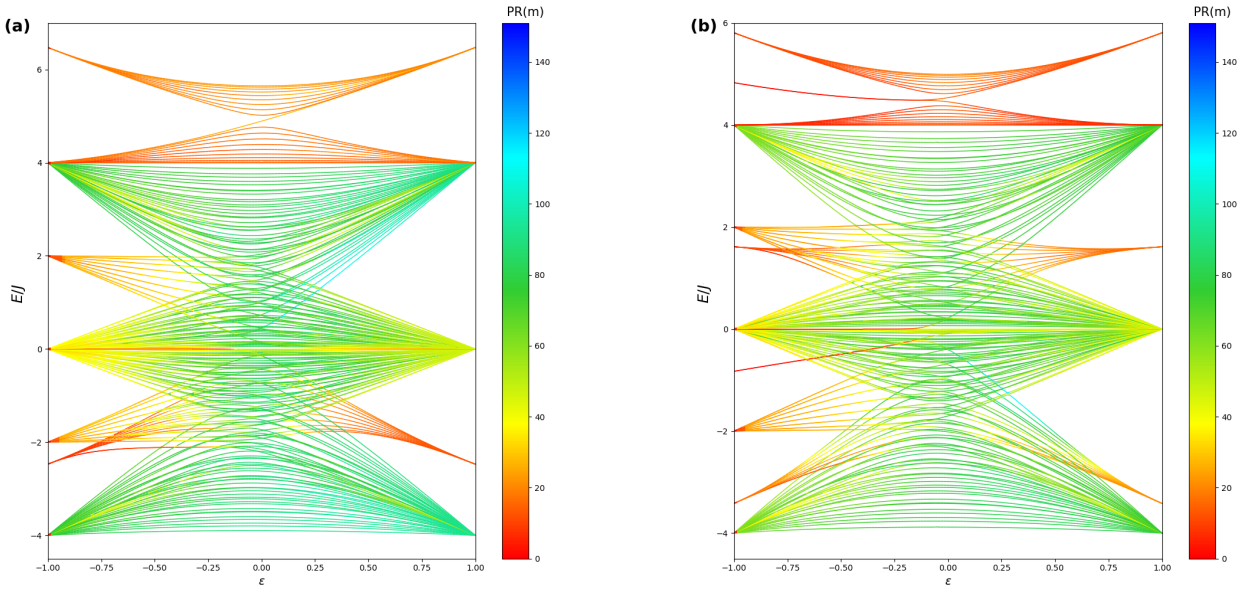

Fig. 3.5: Eigenspectrum of two types of interacting SSH model as ϵ varies between topological to trivial regime for a lattice with $N = 20$. (a) shows the eigenspectrum of the on-site interaction model with $U = 4$. (b) shows the eigenspectrum of the hardcore nearest neighbor interaction model with $V = 4$.

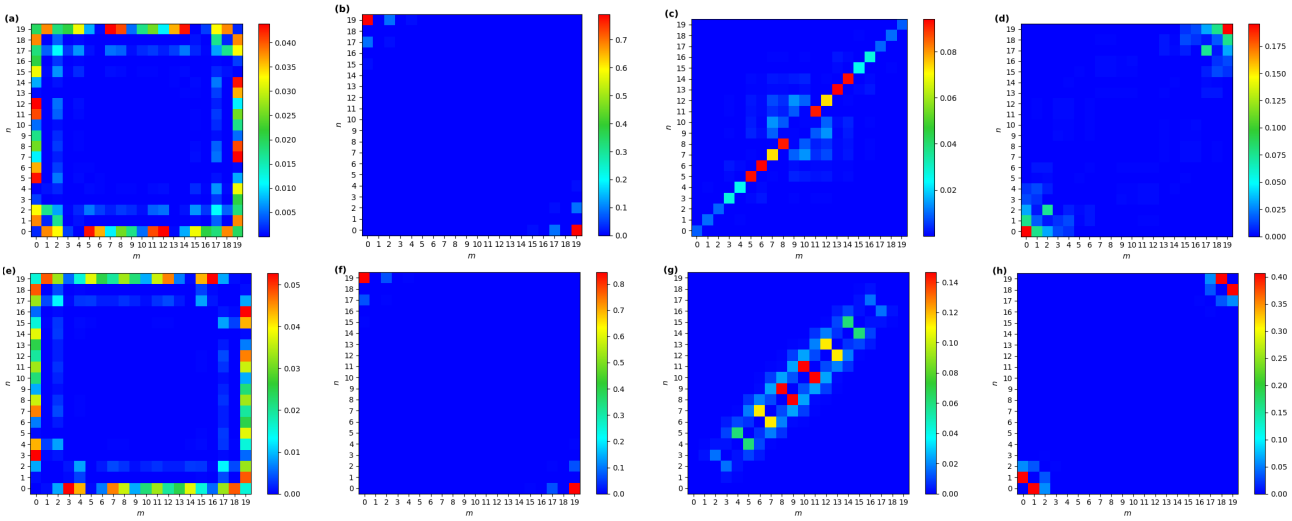

Fig. 3.6: Correlation matrices of eigenstates taken from $\epsilon = -0.5$ cut in the eigenspectrum from Fig.3.5. The colormap in all the plots is the probability $P(m, n)$ of finding a particle in site m and the other at site n. (a)-(d) shows the eigenstates for the on-site interaction model Fig.3.5(a) whereas (e)-(h) shows the eigenstates for the nearest meighbor interaction model Fig.3.5(b)

kinetic energy and bind the particles together although being repulsive in nature. An interesting fact to note in (c) is that it has most of its dominating terms as diagonal terms, meaning the particles tend to be on the exact same site together, thus making the bound pair doublonic in nature[13] and since we have considered hardcore system in (f), we have zero off-diagonals, thus making the bound pair singulonic in nature. Finally, (d) and (h) show us an outcome of both topology and interaction which is bound edge-edge states. These states tend to populate the edges while keeping the particles close together near the diagonals.

3.3 SSH with staggering: The Rice-Mele model

The Rice-Mele(RM) model is an extension of the SSH model with an additional on-site potential that is staggered for every sublattice site. The RM Hamiltonian is given by:

$$\hat{H} = -\sum_i v\left(\hat{a}_i^\dagger \hat{b}_i + \hat{b}_i^\dagger \hat{a}_i\right) + w\left(\hat{b}_i^\dagger \hat{a}_{i+1} + \hat{a}_{i+1}^\dagger \hat{a}_i\right) + \Delta(\hat{n}_{a,i} - \hat{n}_{b,i}) \tag{3.12}$$

Following the approach as the SSH model, we obtain the RM spinor vector and the energy eigenvalues to be:

$$\mathbf{h}(k) = (v + wcos(k))\hat{\mathbf{x}} + wsin(k)\hat{\mathbf{y}} + \Delta\hat{\mathbf{z}} \tag{3.13}$$

$$E_\pm = \pm|\mathbf{h}(k)| \tag{3.14}$$

If we plot the curve in the parameter space, it turns out to be the same loop as in the SSH case, but with an elevation Δ above the z-axis, thus breaking chiral symmetry for non-zero staggering potential.
Fig.3.7 shows different ways by which one can obtain a topological phase transition by moving the momentum states. In the first two methods, we will arrive at some point where one momentum state has to touch the origin. From the chiral symmetry properties of our model, this has to imply gap closing as the energy at the origin is zero. However, in the third method which is possible in the RM model, we can retain a gap throughout the adiabatic process by avoiding the origin and still manage to enter and leave the topological phase.

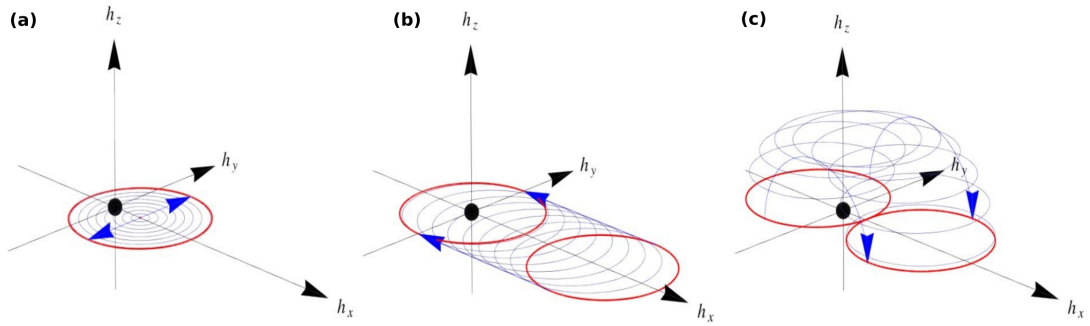

Fig. 3.7: Schematic of how we can go from a trivial to a topological phase. (a) shows the method where we vary w and thus, increase the radius of the momentum loop. (b) shows the method where we change v keeping w constant and thus, shift the circle along the x-axis. (c) is a method where we pick up the loop and move it from the topological regime.[9]

Thus, we can propose schemes where we vary v, w, Δ as a parameter of time and adiabatically evolve the system in a process known as Thouless pumping!

Summary

In this chapter we have analytically shown how topology appears in the SSH model. From our numerical analysis, we have found out that topological phase transition has given rise to edge states that only appear in the configuration that possesses non-trivial topology. We briefly looked into the chiral symmetry of SSH model that prevents adiabatic *trivial* $\leftrightarrow$ *topology* transition, and we have also found a workaround to this by breaking this symmetry in the Rice-Mele model. Finally, we have seen the existence of topology and its signatures in the eigenspectrum of interacting SSH systems also.

Chapter 4

Quantum walks in different models

4.1 QW of bosons with on-site interaction

We have analysed the eigenspectrum of our interacting model by varying the dimerization strength and visualizing various eigenstates that exhibit topological properties in the correlation matrix. Now, we investigate the time dynamics of these edge states via quantum walks with the bosons being initialized at the edge. Fig.4.1 illustrates the quantum walk for various interaction strengths.

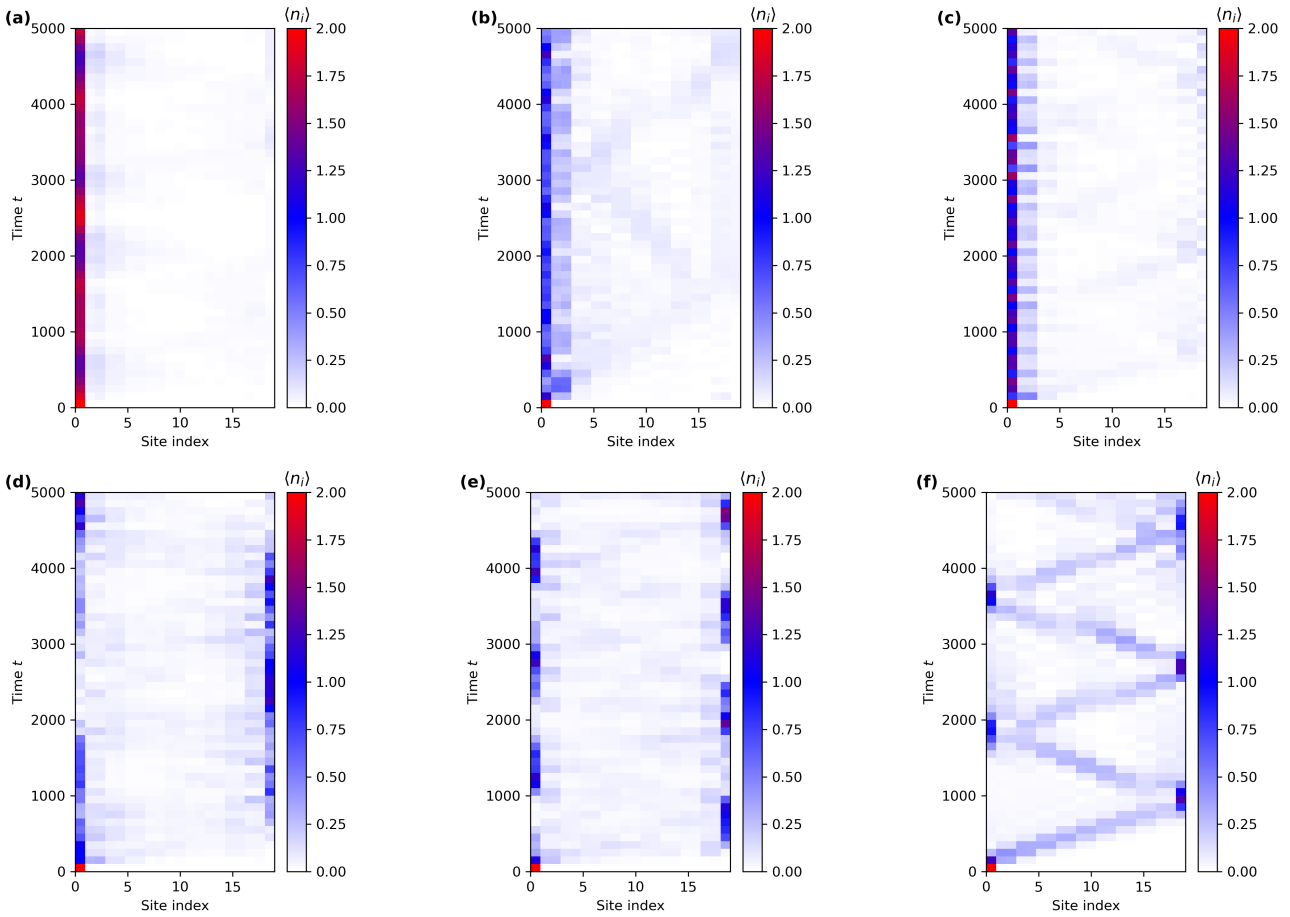

Fig. 4.1: Quantum walk of two bosons initialized at the edge for different values of U. The quantum walk is performed for $v = 0.1$, $w = 1$ with 20 lattice sites. The The values of U for each plot is as follows: (a) $U = 0.2$, (b) $U = 1.0$, (c) $U = 1.8$, (d) $U = 1.85$, (e) $U = 2.0$, (f) $U = 2.5$

We have observed from our QWs that the stability of edge states in the interacting SSH model decreases as the interaction strength U increases, with dissipation into the bulk becoming significant at two critical values: $U = 1$ and $U = 1.85$. At $U = 1$, the particles partially dissipate into the bulk while partially remaining at the edge, while after the energy value crosses $U = 1.85$, both particles gradually lose their edge localization and seep into the bulk. This phenomenon can be attributed to the Fano-Feshbach resonance, where the interaction term creates strong dissipation channels when the bound state band crosses the scattering bands.
Di Liberto has performed analytical calculations on this resonant scattering in a two-particle SSH model with interactions [14], showing that it leads to a strong mixing of scattering states into repulsively bound states and vice versa. Specifically, the narrow bound band becomes an edge-bulk state when it crosses the Type-II scattering band (with one particle at the edge and the other in the bulk) at $U = 1$, and the edge localization disappears completely when the bound band crosses the Type-I scattering band (with strong bulk-bulk scattering) at $U \approx 1.85$. Consequently, although we have observed the existence of edge states in the on-site interacting SSH model, the introduction of interaction leads to the creation of dissipative channels, causing the edge particles to eventually seep into the bulk.

4.2 Mean chiral displacement and the Chern number

We have investigated a dynamic method for adiabatically modifying the Hamiltonian of an interacting system to determine its Chern number. However, recent developments in this field have led to the introduction of mean chiral displacement (MCD), which can be evaluated through quantum walks and converges to the Chern number when its expectation value is calculated with time. Experiments using twisted photons have attempted to characterize topology using MCD for single particle systems[19, 20, 21]. The MCD operator, defined as the product of the chiral operator and the center of polarization, is given by Eq.4.1.

$$\hat{\mathcal{P}} = \hat{\Gamma}.\left(\sum_i \hat{x}_i.\hat{n(x_i)}\right) \tag{4.1}$$

Ostahie *et al.* [22] have shown that the many-body MCD is related to the Chern number by Eq.4.2, where ν is the Chern number as defined in Eq.1.7, and E_k is the energy of the k-th band.

$$\mathcal{P}(t) \simeq \frac{\nu}{2} - \int dk \frac{4}{\pi} \cos\left(2E_k t\right) \left(\boldsymbol{n}_k \times \partial_k \boldsymbol{n}_k\right)_z \tag{4.2}$$

In the limit of large time, the cosine term in the integral tends to zero with small fluctuations, while the first term drives the mean chiral displacement (MCD) to converge to half of the Chern number of the system.
Fig.4.2 displays the time evolution of a single boson quantum walk and the expectation value of $\mathcal{P}(t)$. The MCD oscillates around zero for the trivial dimerization and around 0.5 for the topological dimerization. Fig.4.3 shows the mean chiral displacement of the interacting SSH model for both dimerizations. The topological phase exhibits MCD fluctuations around $\mathcal{P} = 1.32$ for $U = 1$, and $\mathcal{P} = 1.58$ for $U = 5$, while the trivial phase shows MCD fluctuations around $\mathcal{P} \approx 0$ for both U. The fluctuations increase with increased interaction, leading to increased deviation from the actual Chern number value of $\mathcal{P} = 1$ for two bosons performing QW. This deviation may be attributed to the interaction term inducing corrections to the MCD, which overestimates the Chern number calculated by this method. Nonetheless, the

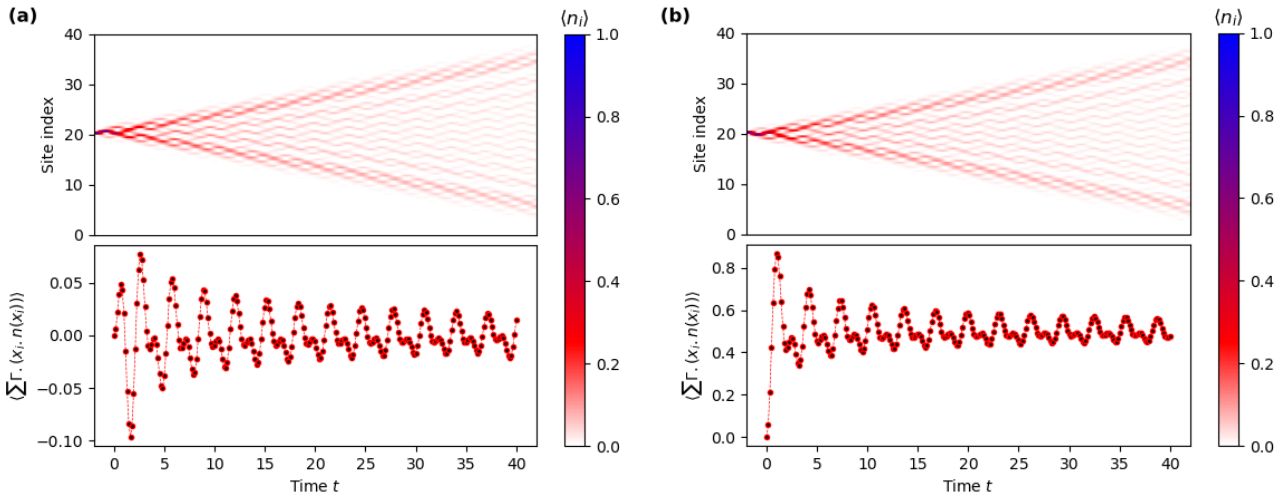

Fig. 4.2: The quantum walk of a single boson in a non-interacting SSH model and its mean chiral displacement for two different lattice dimerizations evolve with time. (a) has $\epsilon = 0.5$ while (b) has $\epsilon = -0.5$.

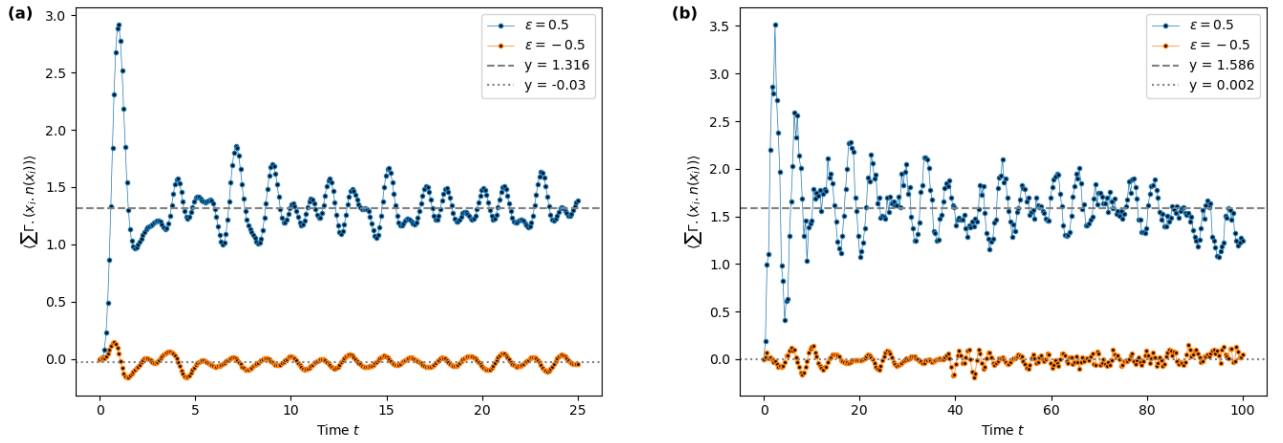

Fig. 4.3: The mean chiral displacement for different interaction values. (a) shows the MCD for both dimerizations of SSH lattice with $U = 1$ while (b) shows MCD for $U = 5$.

mean chiral displacement captures the signature of a non-zero Chern number in our system, indicating that the on-site interaction system preserves topology.

4.3 QW of hardcore nearest neighbor interacting SSH on a quantum computer

Implementing bosonic quantum walk on a quantum computer is a challenging task because each site can accommodate multiple bosons. Ideally, we would require m qudits, each with d dimensions, to simulate a d-boson system on m sites. However, a hardcore bosonic system which behaves like spinless fermions can be mapped to a spin system using the Jordan-Wigner transformation, making it suitable for implementation on a quantum computer.
Smith et al.[23] have proposed a quantum algorithm that uses *Trotterisation decomposition* to

give the time dynamics of a Heisenberg spin model given in Eq.4.3.

$$\hat{H} = -\sum_{n} \frac{J_n^{xy}}{2}(S_n^+ S_{n+1}^- + S_{n+1}^+ S_n^-) + J_n^z S_n^z S_{n+1}^z + h_n S_n^z \tag{4.3}$$

Performing Jordan Wigner transformation of the SSH Hamiltonian in Eq.3.1 assuming $v = J(1+\delta)$, $w = J(1-\delta)$, $U = 0$ and hardcore, the values of the Heisenberg parameters for which both the Hubbard and Heisenberg model give the same physics are:

$$J_n^{xy} = \frac{J}{2}(1 + (-1)^n \epsilon), \qquad J_n^z = \frac{V}{4}, \qquad h_n = \begin{cases} \frac{V}{4} & \text{if } n = 0, N \\ -\frac{V}{4} & \text{otherwise} \end{cases} \tag{4.4}$$

Our nearest neighbor interaction model in quantum computer simulation exhibits a pronounced edge localization, in agreement with the exact results, as illustrated in Fig.4.4. This edge localization is remarkably robust, enduring under strong interaction strengths V with moderate bulk dissipation.

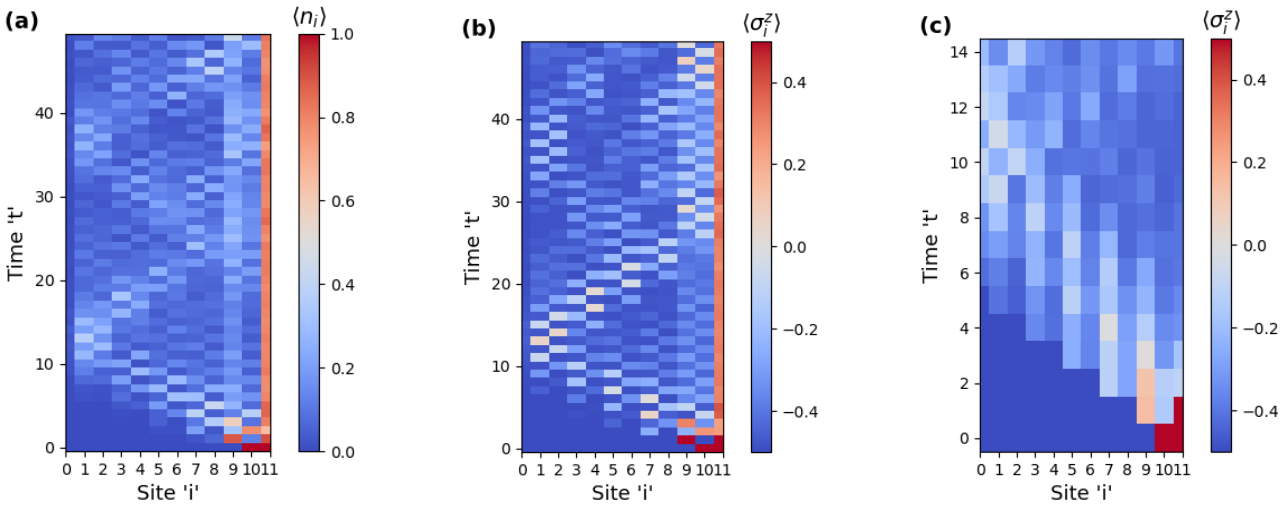

Fig. 4.4: QW of the nearest neighbor interacting SSH model with hardcore bosons on a lattice with $\epsilon = -0.5$, $L = 12$ and $V = 1$. (a) shows the exact result with the colorbar corresponding to the density occupaation of bosons. (b) and (c) are the quantum simulator implementation of the same model with the colorbar representing the average spin of a site where $+0.5$ corresponds to a boson sitting in the site and -0.5 corresponds to no boson at a site. (b) has implemented the QW in 50 trotterization steps whereas (c) has implemented the QW in 15 trotterization steps. We notice that on taking smaller steps, we get erroneous result of time evolution

The correlation matrices in Fig.4.5 reveals the presence of both scattering bulk-edge states and bound bulk-bulk states in interacting systems, as confirmed by the eigenspectrum analysis presented in Fig.3.6. At $t = 3$, the particle begins to transition from the edge to the bulk, exhibiting a preferential motion along the edge and diagonal of the matrix. At $t = 15$ and $t = 48$, the density distribution along the edge and diagonal becomes pronounced, consistent with the existence of scattering bulk-edge states, with only minor contributions from bound bulk-bulk states.

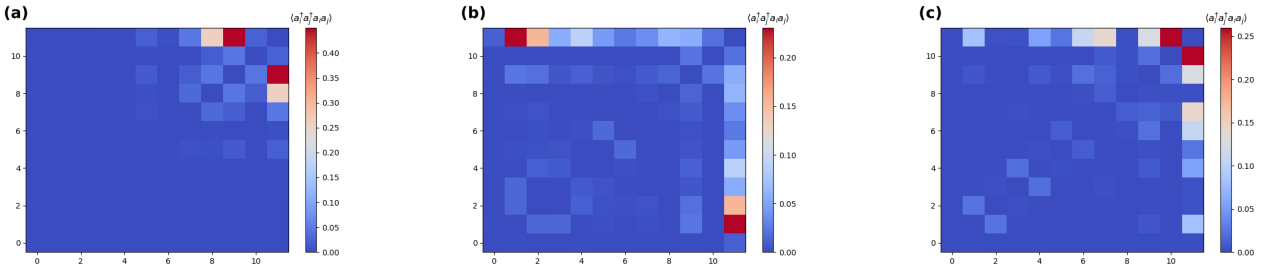

Fig. 4.5: Correlation matrix of the QW as in Fig.4.4(b) at various time steps. (a) is at $t = 3$, (b) at $t = 15$, and (c) at $t = 48$.

4.4 The interacting SSH model with Thouless pumping

Thouless pumping, originally proposed by Thouless [6], is a mechanism that enables quantized charge transport by periodically changing the lattice potentials. When the parameters are slowly varied as a function of time under adiabatic conditions, the system traverses through the entire momentum state of a band. In a single cycle of Thouless pumping, the pumped charge quanta is equivalent to the Chern number[15]. In this study, we implement a numerical scheme that periodically varies dimerization and staggering strength with time, such that the gap closing point is enclosed. We define the time-dependent pumping scheme using the parameters $v = J(1 + \delta)$ and $w = J(1 - \delta)$ as follows:

$$\delta = \delta_0 \cos(\theta(t)) \qquad \Delta = \Delta_0 \sin(\theta(t)) \tag{4.5}$$

where $\theta(t) = \frac{2\pi t}{T}$.

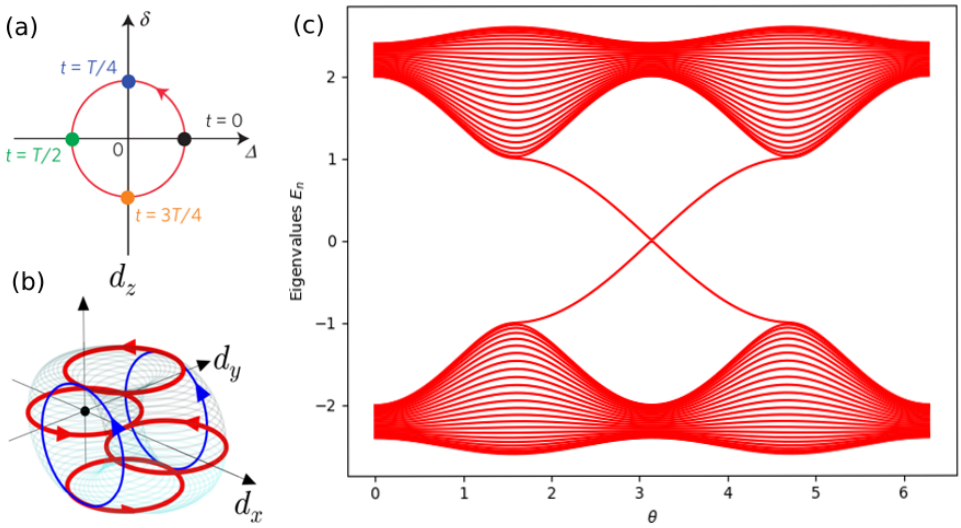

Fig. 4.6: Schematic of thouless pumping. (a) shows the values δ and Δ take in a single cycle[16]. (b) shows how the momentum states move in the parameter space as we implement the pumping[11]. (c) shows the band evolution as we vary $\theta(t)$. We notice that the band remains gapped throughout the pump and the system shifts from a trivial to topological phase and back to its initial state in a single pump.

The quantum walk of two bosons that are initially in the center of a lattice, where both particles occupy the same site, is presented below. We employ our pumping in the softcore on-site interacting SSH model and investigate the possibility of quantifying the Chern number of the system. The staggering and dimerization strengths are modulated as a function of

time, as given by Eq.4.5. The Chern number is determined from the displacement of the particles' center of mass using the formula given in Eq.4.6. We have calculated the Chern

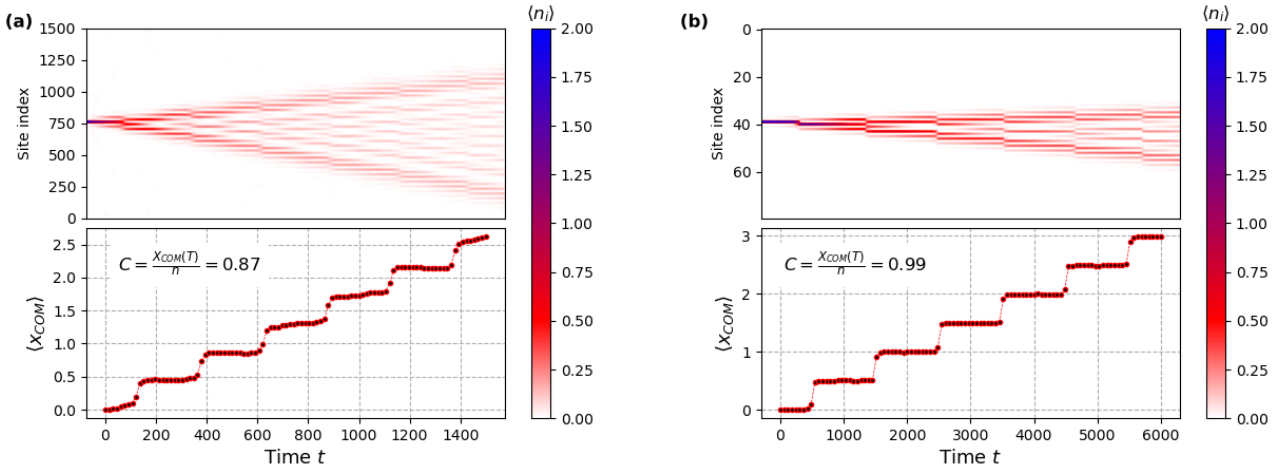

Fig. 4.7: Quantum walk of two bosons in a lattice undergoing Thouless pumping as described in Eq.4.5. (a) has $U = 10$ with pumping period $T = 500$ while (b) has $U = 30$ with pumping period $T = 2000$.

number from the shift in the particles' COM using the formula[17] where:

$$x_{COM}(t) = \frac{1}{2} \frac{\langle \psi(t) | \sum_i \hat{i}.\hat{n}_i | \psi(t) \rangle}{n} \tag{4.6}$$

For our quantum walk, we consider a system with two bosons, and the value of n is accordingly set to 2. The center of mass undergoes abrupt changes whenever the sign of Δ is switched, leading to a quantized charge pumping. We observe two such pumps in a single cycle, with one particle being pumped at each of the two steep shifts in x_{COM}. The Chern number per particle calculated comes out to be $C = 0.87$ for $U = 10$ and $C = 0.99$ for $U = 30$. $U = 10$ deviates more from the expected value due to corrections in the Chern number leading us to measure the *reduced Chern number*[18]. Thus, it gives a dynamic quantification of our system's topology and confirms the on-site interacting SSH model has topology preserved due to inversion symmetry. We notice that the thouless pumping is more pronounced for larger values of U since they aid in stronger localization by creating bound pairs. It is important to note that the duration of pumping must exceed the minimum band gap encountered during the cycle; otherwise, the computed Chern number may deviate significantly from the actual value, despite observing step-like changes in the center of mass.

Summary

In this chapter, we implemented quantum walks to explore the topological features of the SSH model we had introduced in chapter 3. We implemented QW on the on-site interacting SSH model and saw edge states are erased in presence of interaction by causing channels to dissipate into the bulk due even though edge states exist in the interacting SSH energy spectrum. We quantified the Chern number of the on-site interacting SSH model by both dynamically varying varying the Hamiltonian and defining a clever operator extract our Chern number in Thouless pumping and mean chiral displacement respectively. Finally, we implemented the QW of nearest neighbor interacting SSH with hardcore bosons on a quantum simulator and saw edge localization along with partial bulk dissipation as repulsively bound pair.

Bibliography

[1] L. I. Schiff, *Quantum Mechanics*. McGraw-Hill, 3rd ed., 1972.

[2] M. V. Berry, "Quantal phase factors accompanying adiabatic changes," *Proceedings of the Royal Society of London. Series A. Mathematical and Physical Sciences*, vol. 392, pp. 45–57, 1984.

[3] D. J. Thouless, M. Kohmoto, M. P. Nightingale, and M. den Nijs, "Quantized hall conductance in a two-dimensional periodic potential," *Physical Review Letters*, vol. 49, no. 6, pp. 405–408, 1982.

[4] R. Karplus and J. M. Luttinger, "Theory of conductivity of polar crystals," *Physical Review*, vol. 95, no. 5, pp. 1154–1160, 1954.

[5] R. D. King-Smith and D. Vanderbilt, "Theory of polarization of crystalline solids," *Physical Review B*, vol. 47, no. 3, pp. 1651–1654, 1993.

[6] D. J. Thouless, "Quantization of particle transport," *Physical Review B*, vol. 27, no. 11, pp. 6083–6087, 1976.

[7] F. D. M. Haldane, "Model for a quantum hall effect without landau levels: Condensed-matter realization of the "parity anomaly"," 1999.

[8] D. Vanderbilt, "Berry phases in electronic structure theory: Electric polarization, orbital magnetization and topological insulators," in *Modern Techniques for Characterizing Magnetic Materials* (Y. J. Uemura, L. C. Gupta, and W. F. Peck Jr, eds.), pp. 89–113, Springer, 2017.

[9] phyx, "Topological Insulators." https://phyx.readthedocs.io/en/latest/TI/Lecture%20notes/1.html.

[10] N. Batra and G. Sheet, "Understanding basic concepts of topological insulators through su-schrieffer-heeger (ssh) model," 2019.

[11] J. K. Asbóth, L. Oroszlány, and A. Pályi, "The su-schrieffer-heeger (ssh) model," in *A Short Course on Topological Insulators*, pp. 1–16, Cham: Springer, 2016.

[12] D. J. Thouless, "Electrons in disordered systems and the theory of localization," *Physics Reports*, vol. 13, no. 3, pp. 93–142, 1974.

[13] P. M. Azcona and C. A. Downing, "Doublons, topology and interactions in a one-dimensional lattice," *Scientific Reports*, vol. 11, no. 1, p. 12540, 2021.

[14] M. Di Liberto, A. Recati, I. Carusotto, and C. Menotti, "Two-body physics in the su-schrieffer-heeger model," *Physical Review A*, vol. 94, no. 6, p. 062704, 2016.

[15] P. Marra and M. Nitta, "Topologically quantized current in quasiperiodic thouless pumps," *Phys. Rev. Res.*, vol. 2, p. 042035, Dec 2020.

[16] S. Nakajima, T. Tomita, S. Taie, T. Ichinose, H. Ozawa, L. Wang, M. Troyer, and Y. Takahashi, "Topological thouless pumping of ultracold fermions," *Nature Physics*, vol. 12, no. 4, pp. 296–300, 2016.

[17] Z. Tao, W. Huang, J. Niu, L. Zhang, Y. Ke, X. Gu, L. Lin, J. Qiu, X. Sun, X. Yang, *et al.*, "Interaction-induced topological pumping in a solid-state quantum system," *arXiv preprint arXiv:2303.04582*, 2023.

[18] W. Liu, S. Hu, L. Zhang, Y. Ke, and C. Lee, "Correlated topological pumping of interacting bosons assisted by bloch oscillations," *Phys. Rev. Res.*, vol. 5, p. 013020, Jan 2023.

[19] F. Cardano, A. D'Errico, A. Dauphin, M. Maffei, B. Piccirillo, C. de Lisio, and L. Marrucci, "Detection of zak phases and topological invariants in a chiral quantum walk of twisted photons," *Nature Communications*, vol. 8, no. 1, p. 15516, 2017.

[20] M. Maffei, A. Dauphin, F. Cardano, M. Lewenstein, and P. Massignan, "Topological characterization of chiral models through their long time dynamics," *New Journal of Physics*, vol. 20, no. 1, p. 01302, 2018.

[21] A. D'Errico, F. Di Colandrea, R. Barboza, A. Dauphin, M. Lewenstein, P. Massignan, L. Marrucci, and F. Cardano, "Bulk detection of time-dependent topological transitions in quenched chiral models," *Phys. Rev. Research*, vol. 2, no. 2, p. 023119, 2020.

[22] B. Ostahie, J. K. Asbóth, I. Carusotto, N. R. Cooper, M. Gullans, N. Goldman, F. Grusdt, M. Hafezi, D. Jaksch, M. Lewenstein, *et al.*, "Multiparticle quantum walk: a dynamical probe of topological many-body excitations," *arXiv preprint arXiv:2209.03569*, 2022.

[23] A. Smith, M. S. Kim, F. Pollmann, J. Knolle, and I. Lesanovsky, "Simulating quantum many-body dynamics on a current digital quantum computer," *npj Quantum Inf*, vol. 5, no. 1, p. 106, 2019.

Appendices

Appendix A

Quantum circuit to implement quantum walk of hardcore bosons

We closely follow the approach of Smith *et al.*[23] to implement the quantum walk of hardcore bosons by mapping it to a heisenberg spin model defined in Eq.4.3 and Eq.4.4. The trotter decomposition is explained in Fig.A.1. The trotter gate in a single trotter step is given in

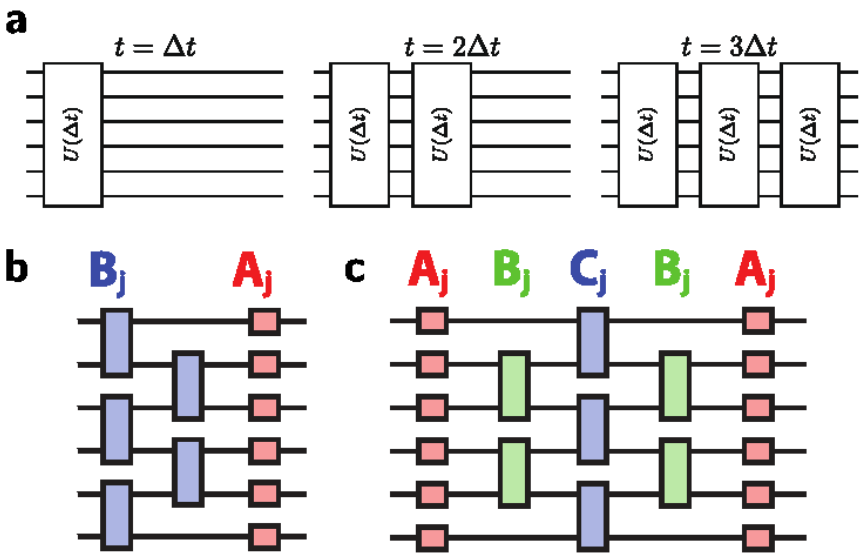

Fig. A.1: Schematic of a trotterizationdecomposition to implement the time evolution of a quantum state. (a) shows addition of trotter steps to implement the time evolution to a time $t = n\Delta t$. (b) shows the simple trotter decomposition of a single trotter step as a combination of single qubit gates A_j and entangling qubit gates B_j while (c) is a symmetric trotter decomposition.

Fig.A.1(b) where the gates:

$$A_j = e^{ih_j\sigma_j^z\Delta t} \tag{A.1}$$

$$B_j = e^{i\left(J_j^z(\sigma_j^z\sigma_{j+1}^z)+J_j^{xy}(\sigma_j^x\sigma_{j+1}^x+\sigma_j^y\sigma_{j+1}^y)\right)\Delta t} \tag{A.2}$$

In terms of the universal $CNOT$ and rotation gates R_x, R_y and R_z along the x, y and z-axis, the gate $B_{i,j}(\alpha, \beta, \gamma)$ is given in Fig.A.2

If we set $\alpha = \beta = -J_n^{xy}\Delta t, \gamma = J_n^z\Delta t$, we have the interaction terms in H being implemented by N as an infinitesimally small unitary rotation between sites i, j.

So, implementing $B_{i,j}(\alpha, \beta, \gamma)$ for both odd and even neighboring sites along with single qubit gates R_z at each site, we will have implemented a single unitary evolution. The quantum circuit for a Heisenberg Trotter step is shown in Fig.A.3

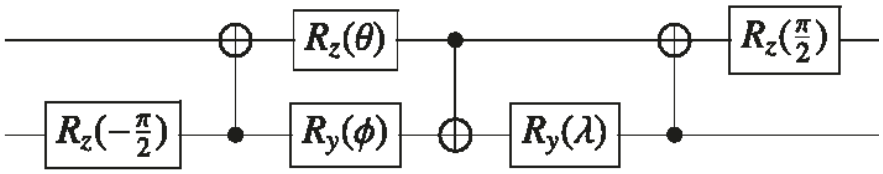

Fig. A.2: The $B_{i,j}(\alpha, \beta, \gamma)$ gate with $\theta = \frac{\pi}{2} - 2\gamma$, $\phi = 2\alpha - \frac{\pi}{2}$, $\lambda = \frac{\pi}{2} - 2\beta$. This is the building block of each entangling gates we impose between neighboring sites to achieve a single trottere step.

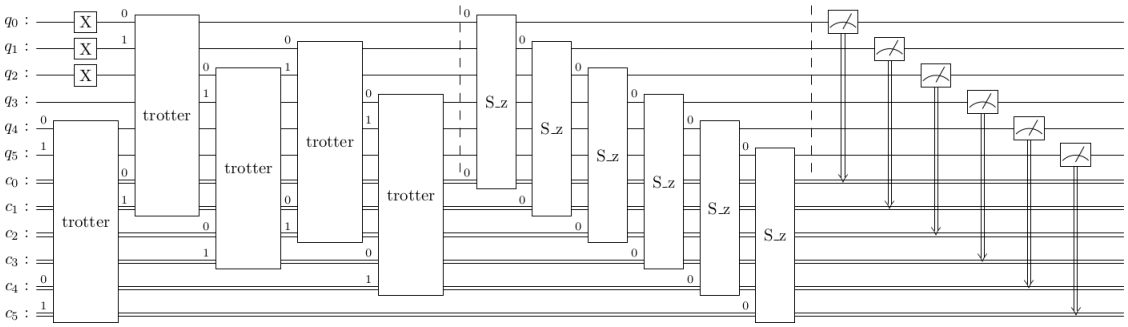

Fig. A.3: The quantum curcuit of a single trotter step in a spin lattice of $L = 6$. The spins are initialized to the domain wall state with half up (using NOT gates) and the other half down. Each gate labelled as "Trotter" is an entangling gate $B_{i,j}(\alpha, \beta, \gamma)$ while the S_z is the R_z gate.

We can initialize a particle at site i by operataing spin i by the NOT gate and flipping the spin to an up spin. If we now substitute the appropriate values of $J_n^{xy}, J_n^z and h_n^z$ as described in Eq.4.4, we will have implemented the quantum walk of hardcore bosons on a spin system.